Talanta 88 (2012) 318–323

Contents lists available at SciVerse ScienceDirect

Talanta

journal homepage: www.elsevier.com/locate/talanta

Sensing behavior of YSZ-based amperometric NO_2 sensors consisting of Mn-based reference-electrode and In_2O_3 sensing-electrode

Han Jin[a], Michael Breedon[b,c], Norio Miura[c,*]

[a] Interdisciplinary Graduate School of Engineering Sciences, Kyushu University, Kasuga-shi, Fukuoka 816-8580, Japan
[b] Japan Society for the Promotion of Science, Tokyo 102-8421, Japan
[c] Art, Science and Technology Center for Cooperative Research, Kyushu University, Kasuga-shi, Fukuoka 816-8580, Japan

ARTICLE INFO

Article history:
Received 19 August 2011
Received in revised form
29 September 2011
Accepted 4 October 2011
Available online 3 November 2011

Keywords:
NO_x sensor
Solid reference electrode
Mn_2O_3
YSZ
In_2O_3

ABSTRACT

Yttria-stabilized zirconia (YSZ)-based amperometric NO_2 sensors comprised of an In_2O_3 sensing-electrode (SE), a Pt counter-electrode (CE) and a Mn_2O_3 reference-electrode (RE) in both tubular and rod geometries were fabricated and their sensing characteristics were examined. For comparative purposes, the performance of the In_2O_3-SE and Pt-CE were also examined against an internal Pt/air-RE. Experimental observations of tubular YSZ-based gas sensors revealed that a three-electrode system exhibited better electrical signal stability, when compared with a two-electrode system. Additionally, replacing the internal Pt/air-RE with an external Mn_2O_3-RE (exposed to the sample gas), was found to have a negligible effect on the gas sensing characteristics of the tubular sensor. This gas sensing equivalence indicates that Mn_2O_3-RE can successfully replace the Pt/air-RE in an amperometric gas sensor. Similarly, rod-type sensors utilizing an In_2O_3-SE and a Mn_2O_3-RE were observed to have almost identical NO_2 sensing characteristics to that of the tubular sensor. Furthermore, both sensors (tubular or rod geometry) exhibited a linear response to increasing NO_2 concentration in the range of 20–200 ppm at 550 °C.

1. Introduction

The anthropogenic emission of nitrogen containing oxides (NO_x) remains a serious problem, as NO_x plays a significant role in the formation of photochemical smog and acid rain [1]. In order to reduce harmful exhaust emissions and to improve fuel efficiency, ultra-lean-burn gasoline vehicles were introduced into the passenger car market [2,3]. In addition, a three-way catalyst (TWC) is typically employed to reduce the levels of air pollutants such as carbon monoxide (CO), hydrocarbons (HCs) and NO_x, although NO_x reduction in the TWC is not favorable at higher O_2 concentrations [4]. To overcome this limitation, selective catalytic reduction (SCR) or lean NO_x trap (LNT) techniques have been proposed [5,6]. However, both of these techniques require on-board NO_x sensors to control either reagent injection (SCR) or trap regeneration (LNT). Therefore, the development of high performance, reliable, and compact sensors is strongly required for the selective and sensitive sensing of NO_x; not only for exhausts applications, but also for environmental monitoring duties.

Several different classes of NO_x sensors are commonly reported in literature [7–10]. Among them, resistance-type sensors utilizing In_2O_3 as a sensing material were reported to have rapid, large and repeatable responses to NO_x [11,12]. However, the selectivity to NO_x remains a challenging issue, particularly limiting the application of this type of sensor for NO_x monitoring in realistic conditions. While, solid-state amperometric sensors have been reported as being highly selective to specific gases, upon the application of an optimum bias voltage [13,14]. Thus, it is reasonable to expect that a sensor utilizing In_2O_3-SE may give acceptable sensitivity and comparatively high selectivity to NO_x under the appropriate biasing conditions.

Recently, we reported on a novel Mn-based solid-state RE (hereinafter denoted as Mn_2O_3-RE) and successfully employed it in YSZ-based oxygen, Lambda (λ) and potentiometric gas sensors [15,16]. However, the sensing characteristics of this novel solid state Mn_2O_3-RE for amperometric sensing applications has yet to be studied.

Thus, in this paper, the gas sensing characteristics of the YSZ-based amperometric gas sensor comprised of an In_2O_3-SE, a Pt-CE and a Mn_2O_3-RE (or inner Pt/air-RE) were examined in either a two or three electrode configuration. The results indicate that a Mn_2O_3-RE can successfully replace the conventional Pt/air-RE in an amperometric NO_2 sensor. Additionally, a compact rod-type YSZ-based gas sensor featuring a three electrode configuration was fabricated, and its sensing performance was measured under identical testing conditions to ascertain the suitability of the Mn_2O_3-RE for miniaturized amperometric sensors.

* Corresponding author. Tel.: +81 92 583 8852; fax: +81 92 583 8976.
E-mail address: miurano@astec.kyushu-u.ac.jp (N. Miura).

0039-9140/$ – see front matter © 2011 Elsevier B.V. All rights reserved.
doi:10.1016/j.talanta.2011.10.047

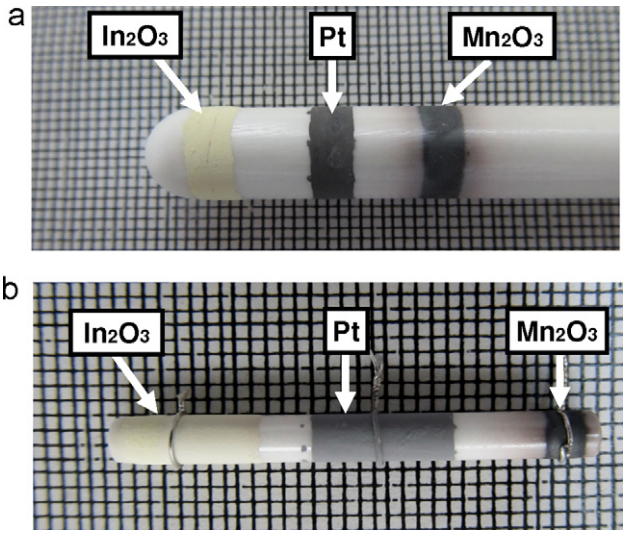

Fig. 1. Photographic images of the fabricated (a) tubular and (b) rod-type YSZ-based sensors (1 mm grid spacing).

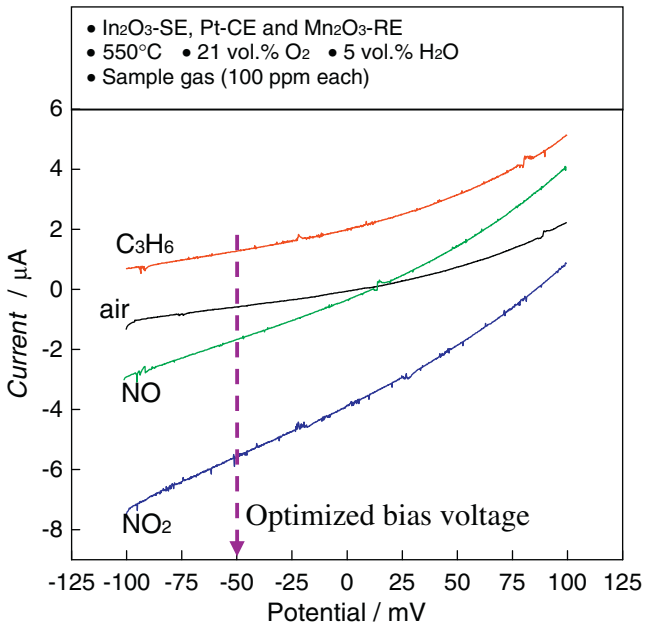

Fig. 2. Polarization curves in base gas (21 vol.% $O_2 + N_2$) or in the sample gas (NO, NO_2 and C_3H_6, 100 ppm each, diluted with the base gas) at 550 °C for the YSZ-based tubular sensor comprised of In_2O_3-SE (calcined at 1200 °C), Pt-CE and Mn_2O_3-RE.

2. Experimental

2.1. Fabrication of tubular and compact rod-type sensors

The electrode configurations of the fabricated tubular and rod-type YSZ-based sensors are presented in Fig. 1(a) and (b), respectively. The tubular and rod-type sensors were fabricated using a commercial hemispherically terminated YSZ tube (300 mm in length, 5 and 8 mm inner and outer diameter, respectively, 8 mol.% Y_2O_3 doped, Nikkato, Japan) and a YSZ rod (30 mm in length and 3 mm in diameter, 8 mol.% Y_2O_3 doped, Nikkato, Japan), respectively. Firstly, commercial Mn_2O_3 powder (99%, Aldrich®, USA) was thoroughly mixed with α-terpineol and the obtained paste was applied by hand-printing on the surface of the YSZ tube or rod to form a Mn_2O_3 layer 3 mm in width. After drying at 130 °C, the YSZ tube or rod coated with the Mn_2O_3 layer was calcined at 1400 °C in air to form the solid-state Mn_2O_3-RE. Subsequently, In_2O_3 powder (99%, Wako Pure Chemical Industries Ltd., Japan) and Pt paste (TR-7601, Tanaka Kikinzoku Kogyo, Japan) were applied on the outer surface of a YSZ tube or rod by hand to form an oxide/metallic layer which was 3 mm in width for the YSZ tube. While, for the YSZ rod, in order to reproduce the same reaction area (75.36 mm^2) with that of the sensor in tubular geometry, an 8 mm-width layer was formed. Following this, the fabricated oxide/metallic layer was calcined to obtain the final In_2O_3-SE and Pt-CE. The calcination temperature for Pt-CE was 1000 °C, while the In_2O_3-SE was calcined over the range of 1000–1400 °C in the intervals of 100 °C. For the tubular sensor, a Pt layer was additionally formed on the internal surface of the end of the YSZ tube, forming a conventional internal Pt/air-RE.

2.2. Evaluation of sensing performance

Considering the intended application of this sensor and the maximum operational temperature of our developed Mn-based RE, an operational temperature of 550 °C was fixed for the measurements of gas-sensing characteristics in a conventional gas-flow apparatus equipped with an electric furnace. The electrodes (In_2O_3-SE, Pt-CE and Mn_2O_3-RE) of the tubular and rod-type sensors were simultaneously exposed to the humidified base gas (21 vol.% O_2, 5 vol.% water vapor, in a balance of N_2) or the sample gas containing one of the following gases: CO, NO, NO_2, H_2, CH_4, C_3H_6, C_3H_8, NH_3; 100 ppm each in humidified base gas. Conversely, the internal Pt/air-RE of the tubular sensor was exposed to the ambient atmosphere (oxygen concentration of 21 vol.%). The sensing signal (electric current) was recorded using an automatic polarization system (Hokuto Denko, HZ-3000) with a constant bias voltage. Here, the gas sensitivity ($\Delta current$) was defined as the difference between the recorded *current* value of the sensor in the sample gas ($current_{\text{sample gas}}$) and that in the base gas ($current_{\text{base gas}}$).

2.3. Characterization of sensing materials

The morphology of the SEs was observed via a field-emission scanning electron microscopy (FE-SEM, JSM-6340F, JEOL, Japan, operating at 10 kV). The current–voltage (polarization) curves were measured with an automatic polarization system (HZ-3000, Hokuto Denko, Japan), employing the linear potential-sweep method at a scan rate of 2 mV/min for a three-electrode configuration at 550 °C in base gas or in sample gas. Impedance characteristics of the sensor were investigated with a complex-impedance analyzer (1255 WB, Solarton, UK) over a frequency range of 0.1 Hz–1 MHz at 550 °C in the base gas.

3. Results and discussion

3.1. Performance of the tubular sensor

Initially, we examined the polarization curves of the sensor consisting of an In_2O_3-SE (calcined at 1200 °C), a Pt-CE, and a Mn_2O_3-RE at 550 °C in humid operating conditions. According to the results reported by other researchers [8,17], the most significant interfering gases during NO_x sensing in exhaust gas are hydrocarbons (e.g., C_3H_6). Therefore, in this study NO, NO_2 and C_3H_6 were selected as the representatives of the target exhaust gas pollutants and interfering species which were examined via polarization curve measurements. From the polarization curve trends (shown in Fig. 2), it can be concluded that the sensor with an In_2O_3-SE (calcined at 1200 °C) at an operational temperature of 550 °C with the application of a bias voltage from −100 mV to 0 mV was a good candidate for NO_2 sensing. In addition, it is apparent that the decrease of the bias voltage

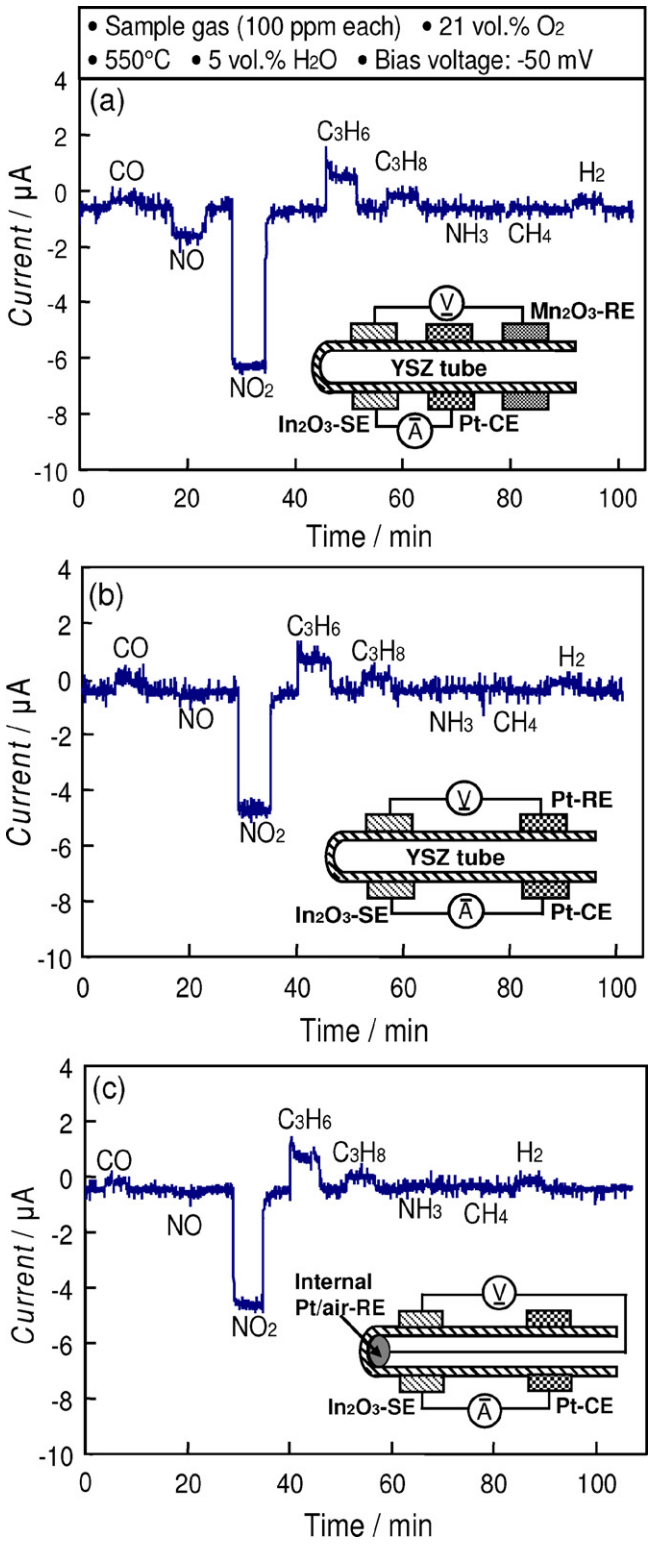

Fig. 3. Gas cross-sensitivity (100 ppm each) at 550 °C for the tubular YSZ-based sensor operating in amperometric mode, comprised of (a) In_2O_3-SE, Pt-CE and Mn_2O_3-RE (three-electrode system); (b) In_2O_3-SE and Pt-CE/RE (two-electrode system), and (c) In_2O_3-SE, Pt-CE and internal Pt/air-RE (three-electrode system).

value towards −100 mV is favorable for increasing sensitivity and selectivity towards NO_2. However, the bias voltage must be carefully selected, lest we shorten the useful operational life of the amperometric sensor. Thus, after considering the selectivity and long-term stability of the sensor, a bias voltage of −50 mV was

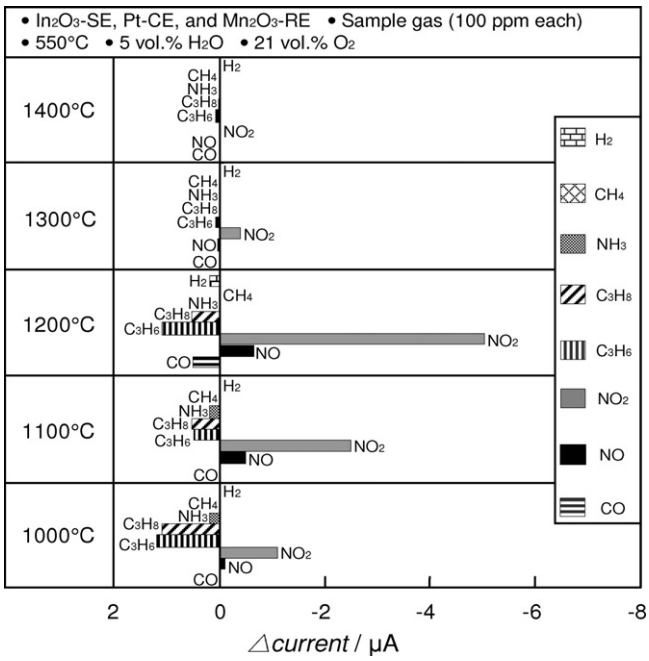

Fig. 4. Comparison of the cross sensitivity towards different gases (100 ppm each) at 550 °C for the tubular YSZ-based sensors comprised of Pt-CE, Mn_2O_3-RE and In_2O_3-SE, calcined at different temperatures.

selected for all gas-sensing measurements. From Fig. 3(a), it can be seen that the sensor consisting of an In_2O_3-SE (calcined at 1200 °C), Pt-CE, and Mn_2O_3-RE exhibited comparatively high selectivity and acceptable sensitivity towards NO_2, with a corresponding $\Delta current$ of −5.1 μA.

In order to compare the sensing performance of the sensor with a two electrode system or three electrode system, the sensor utilizing In_2O_3-SE and Pt-CE/RE (in this configuration, the outer Pt electrode acted as both CE and RE) was also examined, the corresponding response transients are presented in Fig. 3(b). It is apparent that the sensor operating in a two electrode configuration displayed relatively larger signal noise than that of the sensor with a three-electrode system (Fig. 3(a)), indicating that the electrical signal stability of the three electrode system was comparatively better.

For comparison with conventional electrode materials as well as geometric arrangements, the sensing behavior of the tubular sensor with a configuration of an In_2O_3-SE, a Pt-CE and an internal Pt/air-RE was also evaluated, and the obtained result was presented in Fig. 3(c). It can be seen that the sensor employing an internal Pt/air-RE demonstrates similar sensing characteristics with that of the sensor utilizing a Mn_2O_3-RE. Thus, it is clear that Mn_2O_3 can be used for the fabrication of a solid-state RE to potentially replace the conventional Pt/air-RE in YSZ-based amperometric NO_2 sensors with an In_2O_3-SE and Pt-CE.

Based on these results, sensors with a Mn_2O_3-RE, a Pt-CE and an In_2O_3-SE were calcined at different temperatures from 1000 °C to 1400 °C (in intervals of 100 °C) and their cross-sensitivity towards selected different exhaust gas components were examined. The obtained results are presented in Fig. 4. As calcination temperature increased, the selectivity and sensitivity to NO_2 changed drastically, with optimum selectivity and sensitivity recorded for the SE calcined at 1200 °C. Above the calcination temperature of 1200 °C, the sensitivity towards each gas decreased sharply, approaching negligible sensitivity for sensors calcined at 1400 °C. This phenomenon will be discussed in detail in Section 3.3.

Fig. 5 exhibits (a) the *current*–response transients and (b) the dependence of $\Delta current$ on NO_2 concentration in the range

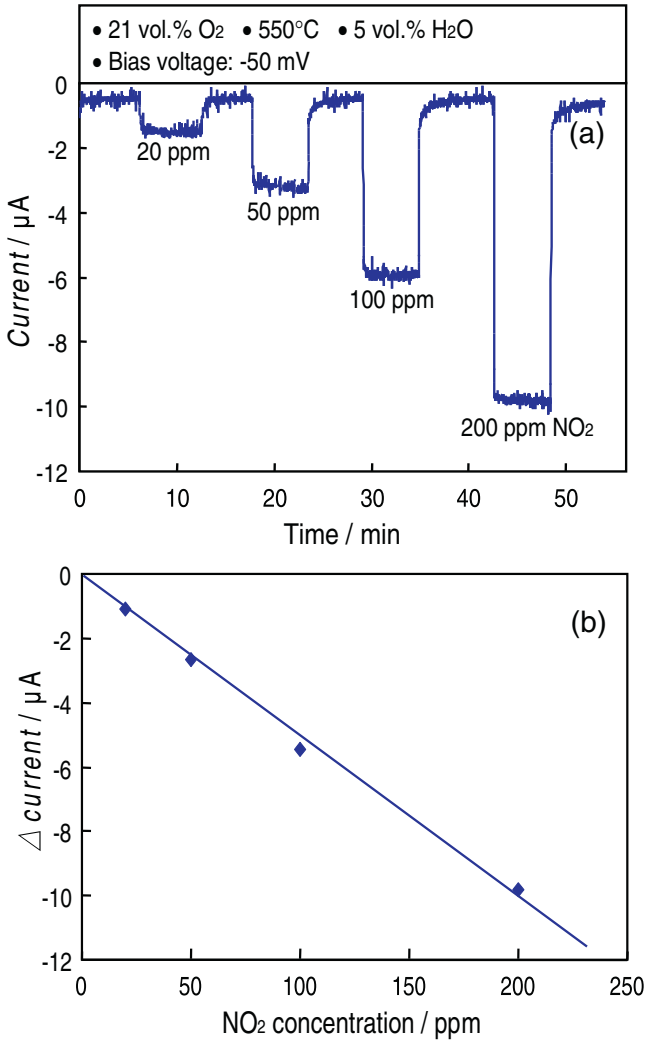

Fig. 5. (a) *Current*–response transients towards different NO_2 concentrations, and (b) the dependence of Δ*current* on NO_2 concentration in the range of 20–200 ppm, for a tubular YSZ-based sensor using In_2O_3-SE, Pt-CE and Mn_2O_3-RE at an operational temperature of 550 °C under humid testing conditions.

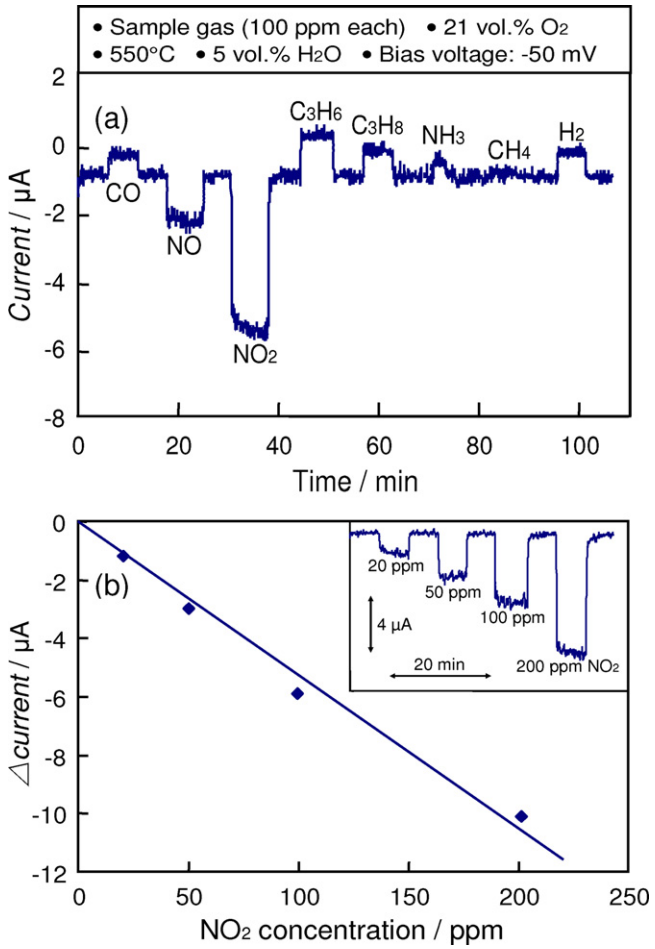

Fig. 6. (a) Cross sensitivity of the rod-type YSZ-based sensor attached with In_2O_3-SE, Pt-CE and Mn_2O_3-RE towards different gases (100 ppm each); (b) *current*–response transients towards different NO_2 concentrations, inset represents the dependence of Δ*current* on the NO_2 concentration in the range of 20–200 ppm at 550 °C.

of 20–200 ppm at 550 °C under humid operation conditions, for the YSZ-based tubular sensor consisting of an In_2O_3-SE, Pt-CE and Mn_2O_3-RE. The *current* of the sensor changed quickly with the increasing change in NO_2 concentration and rapidly reached a steady-state response, with a $t_{90\%}$ response/recovery time of approximately 10 s. Furthermore, Δ*current* varied almost linearly with the NO_2 concentration in the examined range. However, according to stringent emission regulations set worldwide for automobiles, it is still necessary to find methods to increase the sensitivity of our developed sensor towards lower NO_2 concentrations in the future. We expect that since the sensing behavior of the amperometric sensor is governed by Faraday's law, and that the sensing signal of the sensor is proportional to the analyte concentration, a more porous or thin film structure will allow more NO_2 to easily diffuse through the oxide layer and reach the triple phase boundary (TPB). This approach should be helpful to increase the sensitivity of this sensor towards lower NO_2 concentrations.

3.2. Performance of the compact rod-type sensor

Given these findings, we speculated that it maybe possible to use a Mn_2O_3-RE in the fabrication of a miniaturized rod-type amperometric NO_2 sensor consisting of an In_2O_3-SE and a Pt-CE. Therefore, for comparative purposes, the sensing behavior of a compact rod-type sensor comprised of an In_2O_3-SE, a Pt-CE and a Mn_2O_3-RE was evaluated under identical testing conditions. The cross-sensitivity towards different exhaust gases were examined at 550 °C under humid testing conditions, and the obtained results are given in Fig. 6(a). Comparing the NO_2 sensitivity and selectivity of the tubular sensor (as shown in Figs. 3(a) and 5) with those of the rod-type sensor, it is clear that both of the gas sensing performances were almost similar. The sensitivity towards NO_2 was approximately −4.9 µA for the rod-type sensor. Subsequently, the *current*–response transients and the dependence of Δ*current* on the NO_2 concentration in the range of 20–200 ppm at an operational temperature of 550 °C under humid conditions for the compact sensor were also examined (Fig. 6(b)). It is particularly noteworthy that the cross sensitivity and *current*–response transients for both tubular and rod-type sensors were almost identical, indicating that the tubular amperometric sensors can be simplified to a rod geometry, without sacrificing sensing performance, as facilitated by the use of a Mn_2O_3-RE.

3.3. Characterization of the sensing-electrode materials

The morphologies of the In_2O_3-SEs calcined over a temperature range of 1000–1400 °C in increments of 100 °C were observed via SEM, and are presented in Fig. 7(a) and (b). The highly porous structures of the In_2O_3-SEs can be observed from both the

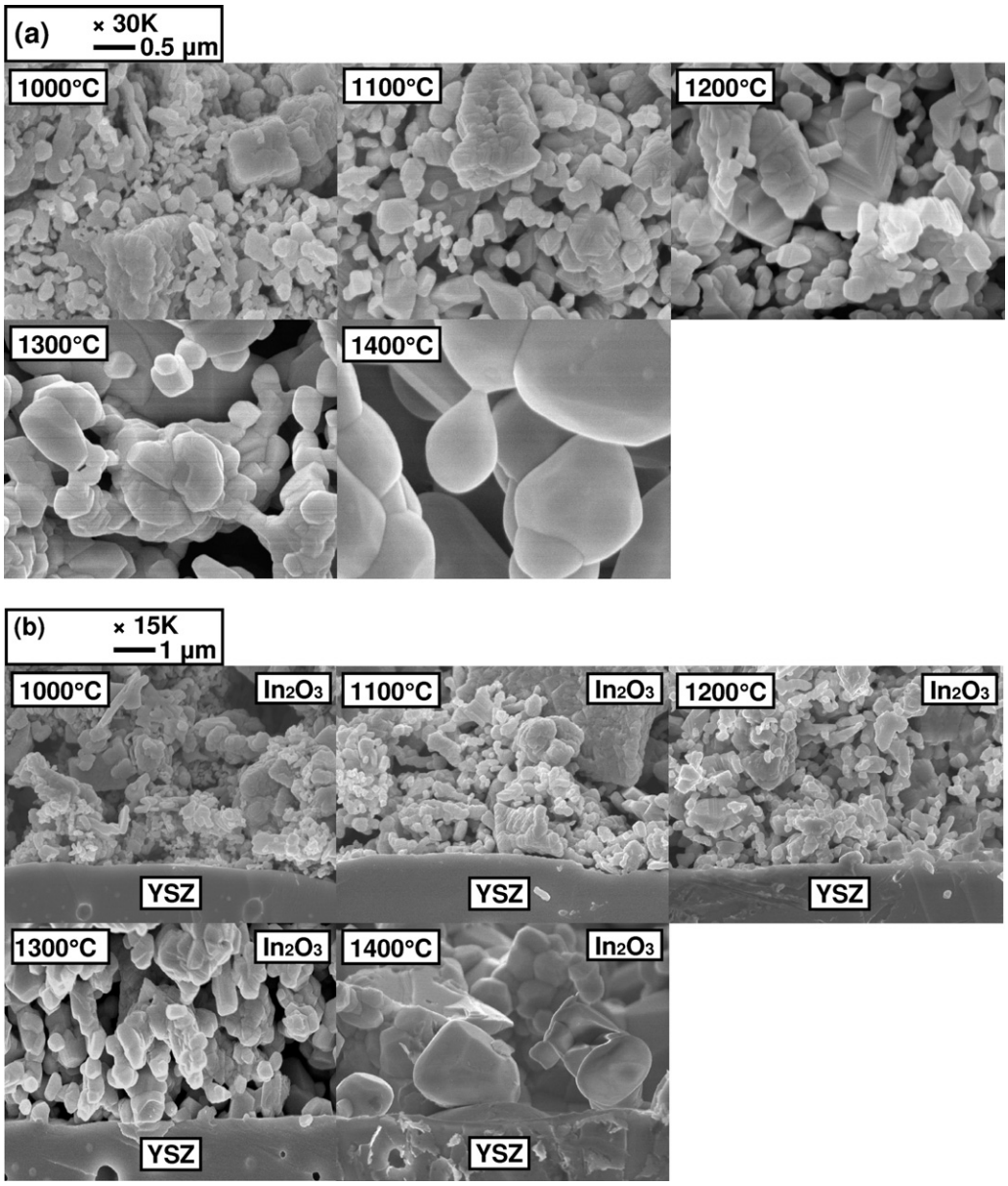

Fig. 7. SEM images of (a) surface of In_2O_3-SE (top view), and (b) YSZ/In_2O_3 interfacial layer (cross-sectional view), after calcination at different temperatures.

surface and cross-sectional images. Additionally, it can be seen that the apparent particle size of In_2O_3-SE increased with increasing calcination temperature. It should be noted that at lower calcination temperatures, the enlargement of the majority of the particles is not apparent, although the size of particles near the interface of the In_2O_3-SE and YSZ slightly increased with increasing calcination temperature. While, at higher calcination temperatures, the particle size increased remarkably. Particularly, after calcination at 1400 °C, the In_2O_3 particles coalesced forming asymmetric particles roughly one order of magnitude larger in size than in the samples calcined at temperatures below 1200 °C. The cross-sectional SEM images (Fig. 7(b)) indicate that at calcination temperatures lower than 1200 °C, the interfacial contact between the In_2O_3–SE and YSZ is relatively poor. While in the sample calcined at 1400 °C, the interface between the In_2O_3-SE and YSZ became increasingly ill-defined, signifying a strong interfacial contact between them. Additionally, the physical contact between In_2O_3-SE particles and YSZ decreased with increasing calcination temperature due to the enlargement of particle size.

Nyquist plots measured in the base gas at 550 °C under humid conditions for the sensors using the In_2O_3-SEs calcined at different temperatures were recorded and the results are presented in Fig. 8. It can be seen that the interfacial (reaction) resistance in the lower frequency range were large and varied significantly with the calcination temperature, particularly, for the SE calcined at 1400 °C which had the largest semicircle. Therefore the total resistance of the sensor at this operational temperature seems to be dominated by the interfacial (reaction) resistance between the SE material and YSZ.

Based on the results of SEM and Nyquist plots presented in Figs. 7 and 8, respectively, the following postulations can be made. It has been well established that, in general, the particle size and interfacial contact of the SE and YSZ can affect the electrochemical catalytic activity significantly. As presented in Fig. 7, it is clear that with an increase in calcination temperature, the morphology of In_2O_3–SE reorganized from a dense tightly packed layer to a more porous structure. It is well known that when the target gas passes over the sintered metal oxide particles of the SE, the

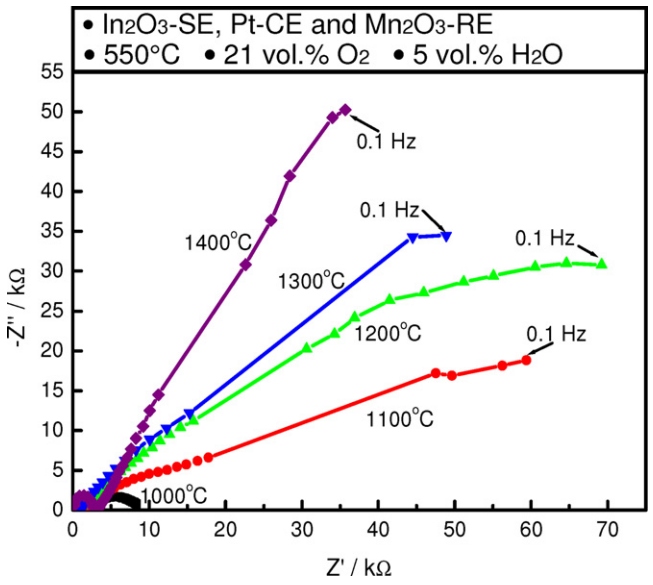

Fig. 8. Nyquist plots of the rod-type YSZ-based sensor consisting of Mn_2O_3-RE, Pt-CE and In_2O_3-SE calcined at temperatures of 1000–1400 °C, examined at 550 °C in the base gas (21 vol.% O_2 and 5 vol.% H_2O).

electrode material often plays a role in the heterogeneous catalysis of the gas mixture. Accordingly, a dense SE layer typically features an extensive network of narrow gas diffusion pathways, formed by heavily packed small particles. Thus, it can be expected that when the sample gas diffuses through the long and narrow physical channels, a significant portion of the sample gas will undergo a catalytically promoted gas-phase oxidation/reduction reaction within the In_2O_3-SE layer, consuming the majority of the target analyte before reaching the desired triple phase boundary (TPB) region. This effect seems to be responsible for the decreasing sensitivity towards testing gases with lowering calcination temperature in the range of 1000–1200 °C. Moreover, it should be considered that the length of the TPB would decrease with increasing particle size. The TPB is an important factor, as this is directly related to the reaction area where important electrochemical reactions occur. As can be seen from the SEM images of Fig. 7, it is clear that the particle size of In_2O_3 calcined at 1400 °C increased largely with respect to other samples, which would suggest a reduction in the available number of reaction sites, owing to the decrease in surface reaction area to volume ratio. In addition, according to the Nyquist plots obtained, the trend of interfacial (reaction) resistance of the In_2O_3-SE was found to increase with increasing calcination temperature over the range of 1000–1400 °C. Hence, it is reasonable to believe that the electrochemical catalytic activity of the SE materials calcined at the temperatures ≥1300 °C should be relatively weaker than that of the SE material calcined at 1200 °C, due to a comparatively smaller number of reaction sites. A weaker electrochemical catalytic activity is most likely the cause of the poor gas sensing performance observed in the In_2O_3-SEs calcined at higher temperatures (≥1300 °C). While the sensing behavior is affected by several variables, which include but are not limited to: SE particle size, SE/YSZ interfacial reaction area (namely, the number of reaction sites), and the porosity of the SE, it can be concluded that the electrode calcined at 1200 °C strikes the optimum balance between the gas-phase oxidation/reduction catalytic activity and electrochemical catalytic activity.

4. Conclusions

The sensing behavior of the tubular sensor consisting of an In_2O_3-SE, a Pt-CE, and a Mn_2O_3-RE (or Pt/air-RE) operating in amperometric mode was evaluated at 550 °C under humid testing conditions. Initially, the amperometric sensing performance of the sensor using a Mn_2O_3-RE was examined in either a two- or three-electrode configuration. It was observed that a two-electrode system gave relatively larger signal noise than that of the sensor configured in a three-electrode system, revealing the superior electrical stability of a three-electrode system. In addition, Mn_2O_3-RE exhibited similar sensing characteristics to the sensor using a conventional Pt/air-RE, highlighting the potential of a Mn_2O_3-RE to replace Pt/air-RE for amperometric sensing applications. According to the gas cross-sensitivity examination, the tubular sensor consisting of a Mn_2O_3-RE, a Pt-CE and an In_2O_3-SE calcined at 1200 °C was recorded the maximum current value of −5.1 μA during exposure to 100 ppm NO_2. Additionally, this kind of amperometric tubular sensor gave a linear *current*–response to NO_2 in a concentration range of 20–200 ppm. The miniaturized rod-type amperometric sensor consisting of an In_2O_3-SE, a Pt-CE, and a Mn_2O_3-RE exhibited almost identical sensing characteristics, when compared with the tubular sensor. Based on the obtained results, it can be concluded that this novel solid-state Mn_2O_3-RE could be potentially utilized in other miniaturized YSZ-based amperometric gas sensors.

Acknowledgements

This work was partially supported by Kyushu University Global-COE Program on “Novel Carbon Resource Sciences” and Grant-in-Aid for Scientific Research (B) (2200353) from JSPS, Japan.

References

[1] Automobile Emissions: An Overview, USA Environmental Protection Agency Office of Mobile Sources EPA 400-F-92-007, 1994, pp. 1–4.
[2] F. Menil, V. Coillard, C. Lucat, Sens. Actuators B: Chem. 67 (2000) 1–23.
[3] N. Docquier, S. Candel, Prog. Energy Combust. Sci. 28 (2002) 107–150.
[4] E. Brich, Y.Y. Wang, J.W. Grizzle, IEEE Trans. Control Syst. Technol. 8 (5) (2000) 767–776.
[5] H. Bosch, F. Janssen, Catal. Today 2 (1988) 369–532.
[6] J.E. Parks, H.D. Ferguson, A.M. Williams, J.M.E. Storey, J.E. Parks, H.D. Ferguson, A.M. Williams, J.M.E. Storey, ASME (ICEF) Conf. Proc., 2004, pp. 153–164.
[7] J. Park, B.Y. Yoon, C.O. Park, W.J. Lee, C.B. Lee, Sens. Actuators B: Chem. 135 (2009) 516–523.
[8] E.L. Brosha, R. Mukundan, R. Lujan, F.H. Garzon, Sens. Actuators B 119 (2006) 398–408.
[9] P. Elumalai, J. Zosel, U. Guth, N. Miura, Ionics 15 (2009) 405–411.
[10] M. Nagao, Y. Namekata, T. Hibino, M. Sano, A. Tomita, Electrochem. Solid-State Lett. 9 (6) (2006) H48–H51.
[11] A.F. Chen, X.D. Huang, Z.F. Tong, S.L. Bai, R.X. Luo, C.C. Liu, Sens. Actuators B 115 (2006) 316–321.
[12] S. Kannana, H. Steinebach, L. Rieth, F. Solzbacher, Sens. Actuators B 148 (2010) 126–134.
[13] J.S. Do, P.J. Chen, Sens. Actuators B 122 (2007) 165–173.
[14] A. Dutta, H. Nishiguchi, Y. Takita, T. Ishihara, Sens. Actuators B 108 (2005) 368–373.
[15] N. Miura, H. Jin, R. Wama, S. Nakakubo, P. Elumala, V.V. Plashnitsa, Sens. Actuators B 152 (2011) 261–266.
[16] H. Jin, V.V. Plashnitsa, M. Breedon, N. Miura, Electrochem. Solid-State Lett. 14 (6) (2011) J23–J25.
[17] R. Mukundan, K. Teranishi, E.L. Brosha, F.H. Garzon, Electrochem. Solid-State Lett. 10 (2) (2007) J26–J29.